Separation of Spacecraft Noise from Geomagnetic Field Data through Density-Based Cluster Analysis and Compressive Sensing

Alex P. Hoffmann[1], **Mark B. Moldwin**[1]

[1]Climate and Space Sciences and Engineering, University of Michigan, Ann Arbor, Michigan

Key Points:

- We present the first use of compressive sensing with cluster analysis to separate spacecraft noise from geomagnetic field data.
- We demonstrate the separation of phase-delayed signals in simulation as well as using residual geomagnetic field data from the SWARM mission.
- The method enables high fidelity magnetic field measurements from resource constrained and magnetically noisy spacecraft such as boomless CubeSats.

Corresponding author: Alex P. Hoffmann, `aphoff@umich.edu`

Abstract

Spacecraft equipped with magnetometers provide useful magnetic field data for a variety of applications such as monitoring the Earth's magnetic field. However, spacecraft electrical systems generate magnetic noise that interfere with geomagnetic field data captured by magnetometers. Traditional solutions to this problem utilize mechanical booms which extend a magnetometer away from noise sources. This solution can exacerbate design complexity and cost of a spacecraft. If a spacecraft is equipped with multiple magnetometers, signal processing algorithms can be used to compare magnetometer measurements and remove stray magnetic noise signals. We propose the use of density-based cluster analysis to identify spacecraft noise signals and of compressive sensing to separate spacecraft noise from geomagnetic field data. This method assumes no prior knowledge of the number, location, or amplitude of noise signals, but assumes that they are independent and have minimal overlapping spectral properties. We demonstrate the validity of this algorithm by separating computer simulated noise signals. We also demonstrate that high latitude magnetic perturbations can be recovered from noisy magnetic field data measured from within the bus of a spacecraft using an experimental CubeSat apparatus. In the case that there are more noise sources than magnetometers, this problem is an instance of Underdetermined Blind Source Separation (UBSS). This work aims to develop a UBSS signal processing algorithm to remove spacecraft noise and eliminate the need for a mechanical boom.

Abstract

Plasma waves in the geospace environment create magnetic fields on the order of 10 nT. This magnitude is well within the range of magnetic noise generated by a spacecraft. We present the application of cluster analysis and compressive sensing to identify and remove spacecraft noise from geomagnetic field data. This method assumes no prior knowledge of the number, location, or amplitude of noise signals, but assumes that they are independent and have minimal overlapping spectral properties. Spacecraft typically have more magnetic noise sources than magnetometers present. This condition makes geomagnetic signal recovery an instance of Underdetermined Blind Source Separation (UBSS). On spacecraft that employ multiple magnetometers, each noise signal appears with a different magnitude and phase at each magnetometer. The magnitude of each noise source at each magnetometer is defined by a wide mixing matrix. In order to separate the geomagnetic signal from noise, we transform the noisy time-domain signals into sparse time-frequency signals using the Non-Stationary Gabor Transform (NSGT). Time-Frequency points which only contain energy from one source signal will draw straight lines in the Time-Frequency domain with slope proportional to the corresponding column in the mixing matrix. Density Based Spatial Clustering of Applications with Noise (DBSCAN) is used to estimate the slope of these lines and recover the mixing matrix. Once the mixing matrix is estimated, compressive sensing is used to reconstruct the time-frequency domain signals with respect to each cluster. The geomagnetic field is assumed to be present equally at each magnetometer, so its phase and magnitude are known a priori. We demonstrate the validity of this algorithm using an experimental CubeSat apparatus and computer simulated noise signals.

Plain Language Summary

Magnetometers are instruments designed to measure magnetic fields. They are used for a variety of purposes such as monitoring the magnetic field of the Earth from a spacecraft. Spacecraft systems such as solar panels and reaction wheels generate magnetic noise that interferes with magnetometer readings. If the spacecraft has multiple magnetometers, each noise source will have a different magnitude at each magnetometer depending on the location of the noise source. The system which describes the magnitude of each noise source at each magnetometer is called a mixing matrix. We propose the use of unsupervised machine learning to estimate the mixing matrix. Once the mixing matrix is estimated, the Earth's magnetic field can be separated from spacecraft magnetic noise using a method called Compressive Sensing.

1 Introduction

Spacecraft equipped with magnetometers can be used to capture in situ measurements of magnetic phenomena in the geospace environment. These measurements are necessary to answer key questions about the nature of the Earth's magnetosphere and its interaction with interplanetary magnetic fields. Understanding how the heliosphere directs the flow of plasma between the Earth and the Sun is critical for a number of applications such as space weather modeling, space exploration, and climate science. A variety of active pursuits employ spacecraft equipped with magnetometers to capture magnetic field data. For example, The European Space Agency's SWARM mission uses a constellation of three satellites to provide high fidelity magnetic field measurements used to model the Earth's magnetic field and study the dynamics of the Earth's core (Fratter et al., 2016). Magnetometers provide invaluable data for space science research, however, the quality of the data is often limited by magnetic noise generated by the spacecraft. Electrical systems aboard a spacecraft generate stray magnetic fields that interfere with magnetic field measurements germane to scientific investigation. The presence of these

stray magnetic fields is a significant obstacle for missions which utilize magnetic field measurements.

On satellites, stray magnetic fields can be generated by subsystems such as solar panels, reaction wheels, battery currents, and magnetorquers. Satellite magnetometers are typically fixed at the end of a mechanical boom to ameliorate the magnitude of noise generated by the spacecraft. For example, the mission SWARM uses two magnetometers mounted on a 4.3 meter boom (McMahon et al., 2013). However, the use of a boom is not always tenable in designs such as rovers and CubeSats where gravity and cost are limiting factors. Booms are also problematic on non-magnetic spacecraft such as DMSP, which is equipped with a tri-axial fluxgate magnetometer on the end of a telescoping boom, but still faces issues with spacecraft noise (Kilcommons et al., 2017).

The use of a single magnetometer on a spacecraft requires characterization of the spacecraft's magnetic signature in order to remove stray magnetic fields. In the case of the spacecraft Cassiope, a software update changed the behavior of the spacecraft fluxgate magnetometer (MGF). Special spacecraft maneuvers to decrease the spacecraft's noise signature were required in order to recalibrate the MGF (Miles et al., 2019). Algorithms to autonomously identify spacecraft noise would allow Cassiopie to do in situ MGF calibration without special spacecraft maneuvers. In spacecraft with multiple magnetometers, Imajo et al. (2021) proposed the use of Independent Component Analysis (ICA) to separate geomagnetic field data, captured by the satellite Michibiki-1, from stray magnetic fields. Imajo et al. (2021) apply ICA by assuming that there is a single geomagnetic field and noise signal for each cartesian axis. This algorithm separates signals based on statistical independence, and works well when the number of noise sources is not more than the number of magnetometers (Naik & Kumar, 2009). Spacecraft typically have an abundance of noise generating electrical equipment, so this condition is rarely met. Sheinker and Moldwin (2016) proposed an analytical method which uses a pair of magnetometers to adaptively cancel magnetic interference without prior knowledge of the noise signal. This method is designed for the case in which a single noise source is present, and does not account for the presence of multiple noise sources. Other methods employ state estimation of the magnetic fields generated by spacecraft subsystems by examining the spacecraft's housekeeping data. Deshmukh et al. (2020) uses a supervised machine learning algorithm in order to estimate the transfer function of housekeeping currents to stray magnetic fields. Total knowledge of the spacecrafts magnetic signature would allow for perfect interference cancellation, however, housekeeping telemetry provides an incomplete image of the spacecrafts current distribution. For low-cost, high volume applications such as CubeSat constellations, it is advantageous to use an algorithm that does not rely on prior knowledge of the spacecraft's magnetic signature or requires human analysis.

In this work, we present the application of the unsupervised machine learning algorithm, Density Based Spatial Clustering of Applications with Noise (DBSCAN), and compressive sensing to separate the geomagnetic field signal from stray magnetic field noise. The separation of geomagnetic signals from stray magnetic fields is an instance of Underdetermined Blind Source Separation (UBSS). UBSS is a class of problems in which there are $B(k) \in \mathbb{C}^m$ listeners and $S(k) \in \mathbb{C}^n$ noise sources, such that $m < n$, which combine in an unknown mixing matrix $\boldsymbol{K} \in \mathbb{C}^{m \times n}$. UBSS is a problem that has been thoroughly researched in other fields such as acoustics and radar signal processing. The system used to model UBSS is defined by the following relationship.

$$\mathbf{B(k) = KS(k)} \tag{1}$$

In the field of acoustics, this problem is famously referred to as the cocktail party problem. In the cocktail party problem, there is a room full of people each having conversations. An array of microphones is placed in the room to record the concurrent con-

versations. The microphone recordings are then used to separate each individual voice. Guo et al. (2017) demonstrate the separation of four human voices using three microphones. He et al. (2021) also demonstrate the separation of six flutes recorded by three microphones using the DBSCAN algorithm.

Due to the spatial structure of magnetic fields, the same algorithms developed to solve UBSS can not be directly applied to magnetic noise cancellation. A magnetic noise signal, s(t), will appear to have a different phase and magnitude at each magnetometer depending on the radial distance and magnetic latitude of the magnetometer with respect to the noise source. In magnetic underdetermined blind source separation, the mixing matrix, K, represents the gain and phase of each signal at each magnetometer. DBSCAN is used to estimate the mixing matrix, K. Once K is known, compressive sensing is used to restore the geomagnetic field signal from the noisy magnetometer data.

We present two experiments to validate this algorithm. The first experiment separates five computer-simulated noise signals. For the second experiment, we use an experimental CubeSat apparatus with copper coil generated signals and three PNI RM3100 magnetometers. The aim of this work is to develop a robust signal processing algorithm to remove spacecraft noise and eliminate the need for a mechanical boom. This work focuses on developing a noise cancellation algorithm for geomagnetic field data, but can also be applied to remove noise in measurements of planetary magnetospheres and interplanetary magnetic fields.

2 Methodology

We apply an iterative approach to identifying spacecraft noise and reconstructing the geomagnetic field signal. Noise signals may be present at different orders of magnitude or frequency spectra. In order to increase the discoverability of a noise signal, we iteratively look at limited frequency bands by using a bandpass filter on the input signals to analyze the signals over a smaller frequency space. Noise signals are identified by transforming the magnetometer data into a sparse domain and clustering the transformed data. After the noise signals are identified, we use compressive sensing to reconstruct the geomagnetic field with the noise signals removed.

2.1 Signal Preprocessing

The separation of magnetic field signals from stray magnetic fields is analogous to a problem thoroughly researched in other fields such as acoustics and is called Underdetermined Blind Source Separation (UBSS). This problem has been heavily investigated for microphone and radar arrays, but the unique structure of a magnetic dipole introduces new complications which have not been well-researched. The placement of magnetometers at different magnetic latitudes makes the magnetic noise signal appear to be phase-delayed, despite mixing instantaneously. As a result, time-frequency domain mixing model, B(t,k) = KS(t,k), can be represented as the following system:

$$\begin{bmatrix} B_1(t,k) \\ B_2(t,k) \\ \vdots \\ B_m(t,k) \end{bmatrix} = \begin{bmatrix} 1 & k_{12}\angle\phi_{12} & k_{13}\angle\phi_{13} & ... & k_{1n}\angle\phi_{1n} \\ 1 & k_{22}\angle\phi_{22} & k_{23}\angle\phi_{23} & ... & k_{2n}\angle\phi_{2n} \\ \vdots & \vdots & \vdots & \ddots & \vdots \\ 1 & k_{m2}\angle\phi_{m2} & k_{m3}\angle\phi_{m3} & ... & k_{mn}\angle\phi_{mn} \end{bmatrix} \begin{bmatrix} S_1(t,k) \\ S_2(t,k) \\ \vdots \\ S_n(t,k) \end{bmatrix} \tag{2}$$

In this mixing system, the geomagnetic source signal we seek to recover, S_1(t,k), is assumed to be identical at each magnetometer a priori. In the geospace environment, this allows us to observe phenomena such as ULF waves which have frequencies less than 5 Hz (Jacobs et al. 1964). The phases, ϕ_{ij}, in the mixing matrix, K, account for the difference of a signal seen by magnetometers at different magnetic latitudes.

Noise signals may be present at different frequency ranges and orders of magnitude. As a result, some signals may interfere with the discovery of other signals. To account for this, we sweep the whole frequency spectrum by iteratively bandpassing the magnetometer signals with overlapping bandpass filters. This allows the algorithm to analyze a much smaller frequency space and improve the identification rate of noise signals.

Once the magnetometer signals, b(t), have been filtered, they are transformed into the Time-Frequency (TF) domain using a Fourier transform in order to increase signal sparsity. Sparsity is a precondition of both mixing matrix estimation and signal reconstruction, however, spacecraft noise signals are not often sparse in the time domain. Typically, the Short-Time Fourier Transform (STFT) is used because signals that are present in multiple time windows will provide more data points to be clustered. In this work, we use the Non-Stationary Gabor Transform (NSGT) to transform magnetometer signals into the Time-Frequency domain. NSGT has advantages over the STFT because it allows the user to evolve the window size with respect to frequency (Jaillet et al., n.d.). As a result, fast and slow frequencies are not limited to the same Window size, and frequency resolution is greatly increased. NSGT also improves the representation of transient signals with respect to traditional transforms. We perform the Non-Stationary Gabor Transform to obtain the UBSS model B(t,k) = KS(t,k). The mixing system of a sparse time-frequency bin where only the signal, S_j(t,k), is present can be defined by a single mixing vector:

$$\begin{bmatrix} \|B_1(t,k)\| \\ \|B_2(t,k)\| \\ \vdots \\ \|B_m(t,k)\| \end{bmatrix} = \begin{bmatrix} k_{1j} \\ k_{2j} \\ \vdots \\ k_{mj} \end{bmatrix} \|S_j(t,k)\| \tag{3}$$

Equation (3) can be rewritten element-wise as:

$$\|S_j(t,k)\| = \frac{\|B_1(t,k)\|}{k_{1j}} = \frac{\|B_2(t,k)\|}{k_{2j}} = ... = \frac{\|B_m(t,k)\|}{k_{mj}} \tag{4}$$

Equation (4) is equivalent to the symmetric form of a line with slope defined by the mixing vector of the noise signal. In order to exploit this relationship, we define a time-frequency space $\mathbf{H} \in \mathbb{R}^{2m}$ in which each the phase and magnitude of the m magnetometer signals is an axis. Sparse TF points will draw straight lines through the origin in the **H**-domain with a slope proportional to the signal's mixing vector.

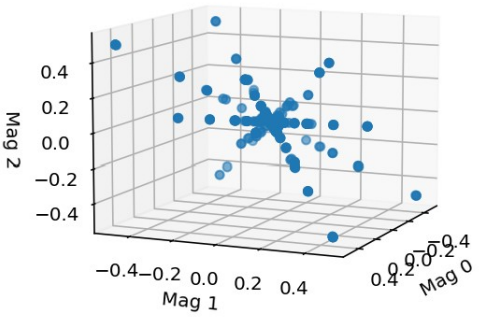

Figure 1. Magnitude subspace of the H-Domain

2.2 Mixing Matrix Estimation

The slope of the lines drawn through the **H**-domain are not easily clusterable in their current form as a collection of scattered data points. We transform the scattered data points in **H**-domain into a clusterable form by projecting the magnitude subspace onto a unit hypersphere (He et al., 2021). Figure 2.2 shows the projected data points of the scattered data in Figure 2.1.

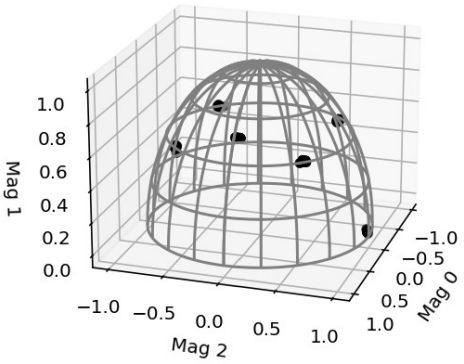

Figure 2. Half Unit-Hypersphere Projection

The **H**-domain magnitude subspace is projected onto a half-unit hypersphere using the following equation.

$$B^*(t,k) = \frac{|B(t,k)|}{\|B(t,k)\|} \tag{5}$$

The majority of the frequency space is filled with negligible energy points that will project randomly onto the unit hypersphere (Sun et al., 2016). We attempt to cleanse the data of these points using a magnitude filter with $\lambda \in (0,1)$:

$$|B(t,k)| > \lambda \cdot \max(|B(t,k)|) \tag{6}$$

The projected data points form tightly clustered groups on the unit hypersphere that will allow us to discover the relative gain between noise signals at different magnetometers. However, we still wish to find the relative phases between noise signals at magnetometers of different magnetic latitudes. To account for this we join each projected time-frequency point to it's relative argument. The relative argument is defined by the following transformation:

$$\arg B(t,k) = \{\, \arg B_j(t,k) - \arg\left(B_0(t,k) \mid j \in [0,m]\right) \} \tag{7}$$

Using the result of Equation 7, we define a new data format H(t,k) by concatenating the projected magnitude data with the argument of the time-frequency data.

$$H(t,k) = (B^*(t,k), \arg\left(B(t,k)\right)) \tag{8}$$

The magnetometer data, H(t,k), is now in a format that can be clustered to discover gain and phase of each signal described in the mixing matrix, K. Figure 3 shows an example of noise signals in a two magnetometer system.

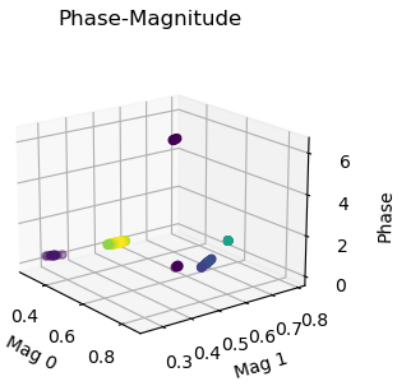

Figure 3. Noise simulated signals recorded by two magnetometers in the H-Space. The horizontal axes are the relative magnitudes projected onto a unit hypersphere. The vertical axis is the relative phase found by Equation 7

Now that the projected magnitude and relative phases are joined, a variety of clustering algorithms can be applied to find the mixing matrix, K. In this work, we use the Density Based Spatial Clustering for Applications with Noise (DBSCAN) algorithm because it does not require user input to discern the number of clusters present, and it will ignore noise points (Ester et al. 1996). DBSCAN has two essential parameters, *eps* and *minPts*, that allow this functionality. The maximum distance for two points to become *neighbors* is the value, *eps*. If a point has *minPts* number of neighbors, it is called a core point. Core points are used to define each cluster. If a point is more than *eps* distance away from any point in a cluster, it is labeled as noise. We use DBSCAN to cluster H(t,k) and use each clusters centroid as the noise signal's mixing vector.

2.3 Signal Reconstruction

Compressive sensing is a method used to reconstruct sparse signals with a sampling rate below two times a signal's bandwidth (Baraniuk, 2007). Reconstructing a signal of length N from a sampled signal of length M, where $M < N$, is an analogous problem to Underdetermined Blind Source Separation. Ordinarily, the system $b = Ks$, where K is a wide matrix, has infinitely many solutions because if $b = Ks$ is a solution, $b = K(s+s')$ is also a solution for any vector s' in the null space of K. Compressive sensing can exactly recover sparse signals and approximate near-sparse signals through minimizing the L1 norm of S with respect to $b-Ks < \varepsilon$. The algorithm works with $O(N^3)$ complexity.

We use CVXPY, A Python-Embedded Modeling Language for Convex Optimization (Diamond & Boyd, n.d.), to reconstruct the signals with the estimated mixing matrix, K. The constraint used to recover the signal, s, from b is:

$$\begin{aligned} &\text{Minimize} && \|s\|_1 \\ &\text{Subject to} && Ks = b \end{aligned} \tag{9}$$

This system is solved using the convex optimization algorithm, Embedded Conic Solver (Domahidi et al., 2013).

3 Experimental Data and Results

We test the proposed method of signal and noise separation through two experiments. The first experiment demonstrates the separation of computer simulated signals using virtual magnetometers. The second experiment demonstrates the separation of SWARM magnetic field data from real magnetic noise signals generated with copper coils. The coil-generated magnetic fields were measured using the PNI RM3100 magnetometer (Regoli et al., 2018).

Figure 5 details the process of identifying noise signals and reconstructing the ambient magnetic field. First (i), the signal offsets are substracted to center the signals around 0 nT. Second (ii), the signals are bandpassed so the algorithm can analyze a more limited frequency range. Third (iii), the signals are transformed into the time-frequency domain using the Non-Stationary Gabor Transform to increase signal sparsity. Fourth (iv), low energy points are filtered out using Equation 6. Fifth (v), the signals are transformed into H(t,k) by projecting the magnitude, $|B(t,k)|$ onto the unit hypersphere and concatenating it with the phase, $\arg B(t,k)$, via Equations 5, 7, and 8. Sixth (vi), the data, H(t,k), are clustered using DBSCAN and the cluster centroids are found. This process loops back to step 2 (ii) until the whole frequency spectrum has been swept. Finally, in the last step (vi), compressive sensing is used to reconstruct the ambient magnetic field. The minimum magnitude, λ in step 4 (iv), and the parameters eps and MinPts in step 6 (vi) may need to be adjusted depending on the length and magnitude of the signals being analyzed.

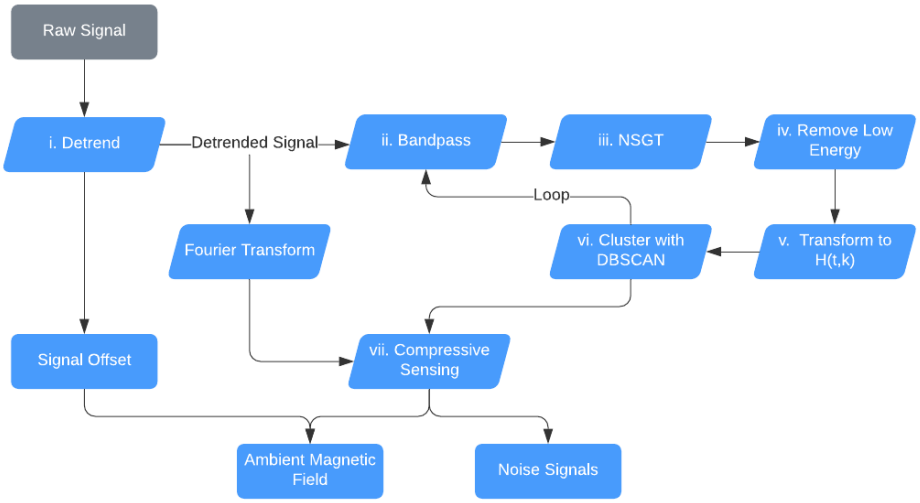

Figure 4. Flow of processes involved in using cluster analysis to discover noise signals and compressive sensing to separate the ambient magnetic field from noise signals.

We evaluate the separation of noise signals via three metrics. The first metric is the Pearson Correlation Coefficient. This measurement gives the covariance between the normalized input and recovered signals.

$$\rho = \frac{\sum_{i=0}^{N-1}(x_i - \bar{x})(y_i - \bar{y})}{\sqrt{\sum_{i=0}^{N-1}|(x_i - \bar{x})|^2 \sum_{i=0}^{N-1}|(y_i - \bar{y})|^2}} \tag{10}$$

The second metric evaluated is the root mean squared error (RMSE). This metric is proportional to the magnitude of the squared error. As a result, the RMSE is very sensitive to large errors.

$$RMSE = \sqrt{\frac{\sum_{i=0}^{N-1}(x_i - y_i)^2}{N}} \tag{11}$$

The final metric is the normalized RMSE (NRMSE). This metric yields the RMSE as a percentage of the magnitude of the signal being measured. It is used to compare the relative error between signals on different orders of magnitude.

$$NRMSE = \frac{RMSE}{|y_{max}|} \tag{12}$$

3.1 Experimental 1: Computer Simulation

In this experiment, we use five simulated source signals, $s(t) = [s_1(t), s_2(t), s_3(t), s_4(t), s_5(t)]$, and three virtual magnetometers $b(t) = Ks(t) = [b_1(t), b_2(t), b_3(t)]$. The proposed algorithm detailed in Figure 4 is tested on 100 seconds of generated data. The signals are combined through the complex mixing matrix in Equation 13 with phases given in radians.

$$K = \begin{bmatrix} 1\angle 0 & 0.83\angle 0 & 0.56\angle 0 & 0.68\angle 0 & 0.30\angle 0 \\ 1\angle 0 & 0.50\angle 1.57 & 0.79\angle 0.523 & 0.29\angle 2.35 & 0.30\angle 0.314 \\ 1\angle 0 & 0.24\angle 1.04 & 0.24\angle 1.04 & 0.68\angle 3.14 & 0.90\angle 0.523 \end{bmatrix} \tag{13}$$

The values in the first column represent the ambient magnetic field signal which appears identically at every magnetometer. Figure 5 shows the five noise sources of varying magnitudes used in this simulation. Three of the signals are sine waves with frequencies of 0.9 Hz, 2 Hz, and 5 Hz. Sine waves are sparse signals that can be represented by a single point in the frequency domain. This makes them easily identifiable by cluster analysis. The two remaining signals used are a sawtooth wave with a frequency of 0.1 Hz, and a square wave with a frequency of 3.0 Hz. These signals inhabit a broad frequency spectrum and diminish the sparsity of the mixed signals.

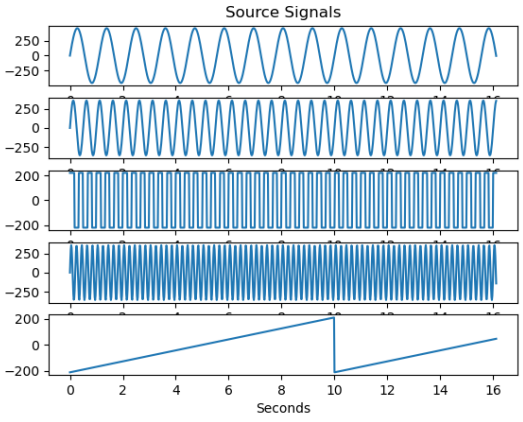

Figure 5. Five computer generated signals.

The signals are combined in the the mixing system $b(t) = Ks(t)$ with the mixing matrix K from equation 13. The resulting signals are sampled by the virtual magnetometers at a rate of 50 samples per second. A random normal signal with a standard deviation of 6 nT is added to each magnetometer signal in order to simulate instrument noise. Figure 6 shows the sampled signals.

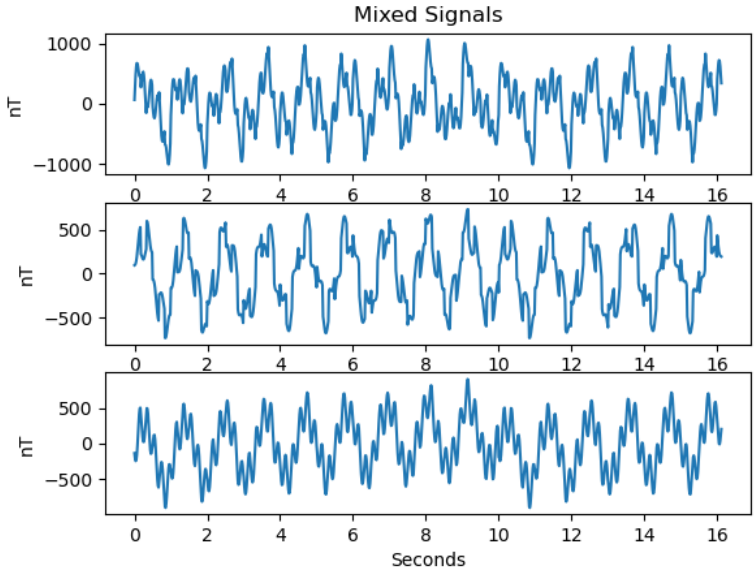

Figure 6. Three magnetometer signals resulting from mixing five source signals in Figure 5.

Following the procedure in Figure 4, the signals were detrended and bandpassed with frequency ranges of [0.01 Hz, 2.12 Hz] and [0.15 Hz, 25 Hz]. Overlapping frequency ranges are analyzed to discover signals that may appear in multiple frequency bands. The signals were then transformed into the Time-Frequency domain using the NSGT. The NSGT is a type of constant-Q transform, so it requires the parameter Q which specifies window size. In this experiment, we used $Q = 12$. In step 4, low energy points were removed using a $\lambda = 0.05$. The resulting data were transformed into H(t,k) and clustered by DBSCAN with parameters $eps = 0.3$ and $MinPts = 3$. These parameters were optimized experimentally using trial and error, however it may be possible to automate parameter selection based on the signals being analyzed. With this configuration, DBSCAN discovered the following five clusters shown below in the columns of $\hat{K}$.

$$\hat{K} = \begin{bmatrix} 1\angle 0 & 0.32\angle 0 & 0.83\angle 0 & 0.56\angle 0 & 0.66\angle 0 \\ 1\angle 0 & 0.32\angle 0.36 & 0.50\angle 1.58 & 0.79\angle 0.52 & 0.30\angle 2.43 \\ 1\angle 0 & 0.90\angle 0.60 & 0.23\angle 1.07 & 0.23\angle 1.07 & 0.69\angle -3.12 \end{bmatrix} \tag{14}$$

Note that the columns of $\hat{K}$ do not match the order of columns of the K detailed in equation 13. The columns of $\hat{K}$ appear in the order in which they are discovered by DBSCAN. However, the mixing matrix discovered by $\hat{K}$ closely matches the gains and phases of the original mixing matrix.

Finally, in step 7, the mixed signals were separated by compressive sensing using the recovered mixing matrix, $\hat{K}$, in Equation 15. The data, H(t,k), are discarded and the raw fourier transform of the mixed signals is separated using the ECOS algorithm. The reconstructed signals are shown in Figure 7.

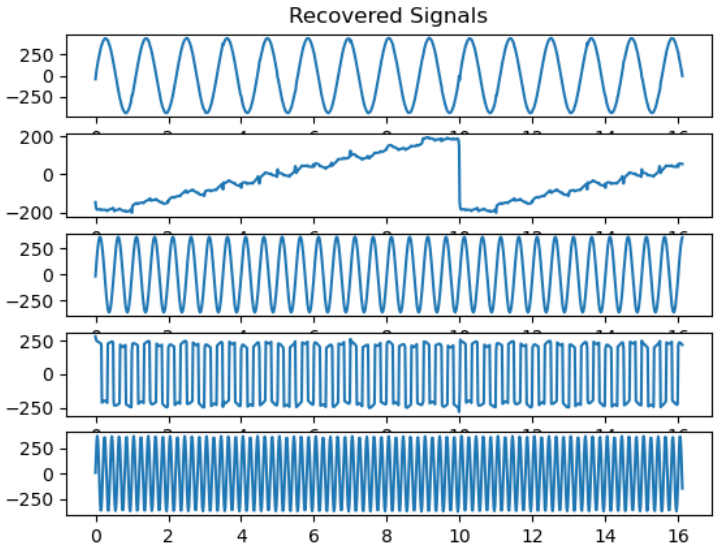

Figure 7. Five reconstructed input signals

The reconstructed signals resemble the original signals with some additional error. In order to evaluate the reconstruction noise, the Pearson Correlation Coefficient, RMSE, and NRMSE of each signal is calculated. The results are shown in the following table.

Metrics					
	Sine A	Sine B	Square	Sine C	Sawtooth
ρ	0.9998	0.9999	0.998	0.9999	0.9939
RMSE	11.28 nT	2.751 nT	14.17 nT	7.995 nT	13.37 nT
NRMSE	2.48%	0.76%	5.06%	2.23%	6.19%

3.2 Experimental 2: Magnetic-Coil Generated Signal Separation

In this experiment, we demonstrate the utility of the proposed algorithm on real magnetic field data. We use three PNI RM3100 magnetometers to record copper coil-generated noise signals. Four copper coils are are driven by signal generators to create the source signals, $s(t) \supset [s_2(t), s_3(t), s_4(t), s_5(t)]$. The signals are combined in the unknown mixing system, $b(t) = Ks(t) = [b_1(t), b_2(t), b_3(t)]$. An artificial signal, $s_1(t)$, is added to each magnetometer signal, $b(t)$, to simulate the presence of the geomagnetic field. The signal, $s_1(t)$, is residual magnetic field data created by subtracting data generated by the IGRF model from magnetic field data measured by SWARM. This process removes the background magnetic field and leaves only magnetic perturbations present in the magnetosphere. The data used in this process were measured by the SWARM A satellite on March 17th, 2015 between 8:53 am and 8:55 am UTC. This part of the orbit passes between the 69th and 76th parallel south and was selected to capture magnetic perturbations in the southern auroral zone.

The proposed algorithm detailed in Figure 4 is tested on 100 seconds of generated data. The signals, $s_2(t)$ and $s_3(t)$, are sine waves with frequencies of 0.4 Hz and 0.8 Hz. The signals, $s_4(t)$ and $s_5(t)$, are square waves with frequencies of 1 Hz and 2 Hz. The three PNI RM3100 magnetometers and four copper coils are placed on the CubeSat ap-

paratus as shown in Figure 8. This experiment was performed in a copper room lined with mu-metal in order to screen out magnetic fields from the surrounding environment.

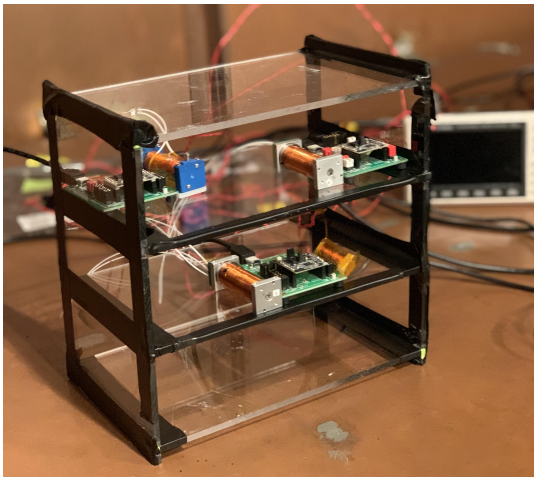

Figure 8. Mock CubeSat Apparatus with three PNI RM3100 Magnetometers and four copper coils driven by signal generators. The Apparatus is placed inside a mu-metal lined copper room that acts as a large magnetic shield can.

The PNI RM3100 is a magneto-inductive magnetometer that measures the magnetic field by counting hysteresis loops with a comparator circuit, called a Schmitt Trigger, and an ASIC. The ASIC records magnetic field measurements by adding to a register every time the Schmitt trigger is saturated. This measurement renders the magnetic field when integrated with respect to time. The ASIC has a cycle count register that controls how many clock cycles pass between integrations. The error of the magnetometer will change with respect with the cycle count. In this experiment, each magnetometer is sampled at a rate of 50 Hz with a cycle count of 200 cycles. The PNI RM3100 is rated to have an error of 6 nT in this configuration. The mixed signals recorded by the PNI RM3100 magnetometers are shown in Figure 9 below.

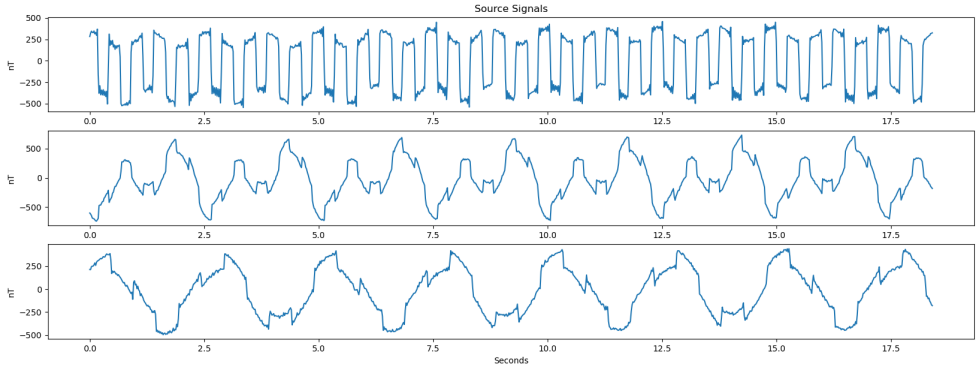

Figure 9. Three mixed signals recorded by PNI RM3100 magnetometers. The five signals present are two sine waves, two square waves, and the added residual magnetic field data.

The algorithm was run on this data following the same steps as in Figure 4 and Section 3.1. The signals were detrended and bandpassed with frequency ranges of [0.01 Hz, 0.51 Hz], [0.07 Hz, 3.76 Hz], and [0.51 Hz, 25 Hz]. The signals were then transformed into the Time-Frequency domain using the NSGT with a quality factor of $Q = 10$. In step 4, low energy points were removed using a $\lambda = 0.09$. The resulting data was transfomed into H(t,k) and clustered by DBSCAN with parameters $eps = 0.3$ and $MinPts = 3$. DBSCAN discovered the following five clusters shown below in the columns of $\hat{K}$.

$$\hat{K} = \begin{bmatrix} 1\angle 0 & 0.023\angle 0 & 0.22\angle 0 & 0.93\angle 0 & 0.02\angle 0 \\ 1\angle 0 & 0.55\angle 1.31 & 0.97\angle 3.09 & 0.35\angle 3.04 & 0.04\angle 6.04 \\ 1\angle 0 & 0.79\angle 4.58 & 0.001\angle 2.94 & 0.15\angle 0.255 & 0.82\angle 2.84 \end{bmatrix} \tag{15}$$

The PNI RM3100 magnetometer was experimentally found to have a lower noise floor when sampled at a higher rate and decimated to a lower rate versus only being sampled at a lower rate. We evaluated this effect by testing step 7, signal reconstruction, on the original 50 Hz data, 10 Hz and 1 Hz data attained through downsampling, and 50 Hz data averaged with a moving mean (N = 10). These signals were separated via compressive sensing using the recovered mixing matrix, $\hat{K}$, in Equation 15. The four reconstructed noise signals from the 50 Hz raw data are shown in Figure 10.

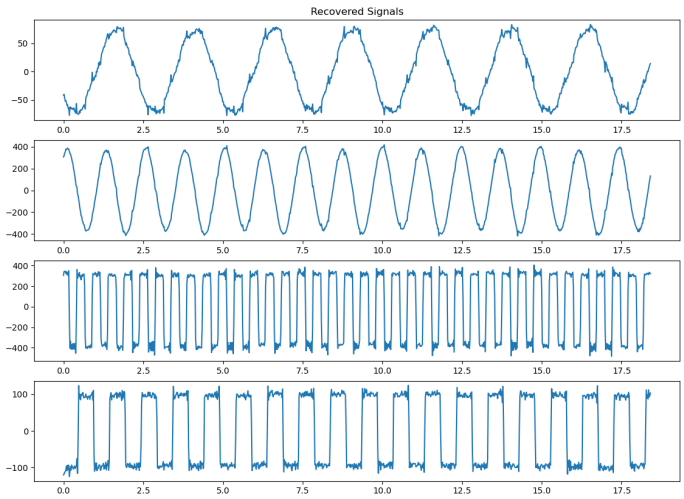

Figure 10. Reconstructed Sine and Square wave signals from 50 Hz mixed signals in Figure 9.

The reconstructed coil-generated signals closely resemble square and sine waves with some additional noise. The recovered residual magnetic field data are shown in Figure 11. The recovered signal is overlayed with the true residual magnetic field signal. The residual data in Figure 11 was reconstructed using the mixed signals decimated to a sampling rate of 10 Hz.

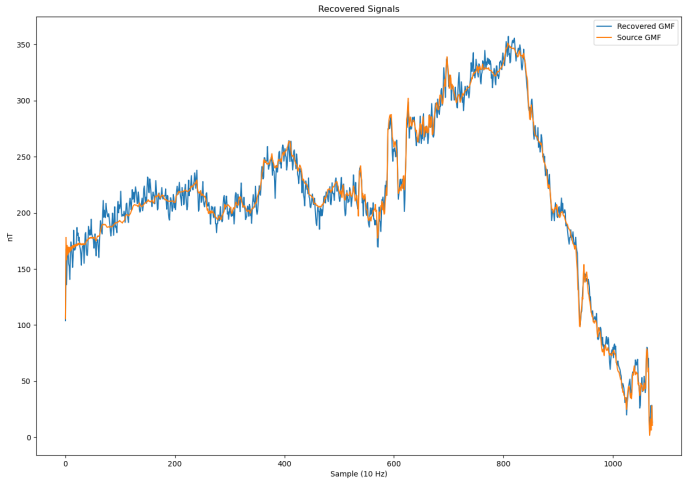

Figure 11. True magnetic perturbation data in orange versus the recovered magnetic perturbation signal in blue. The signal was reconstructed using the mixed signals in figure 9 decimated to a sampling rate of 10 Hz.

The reconstructed signal closely follows the true geomagnetic perturbation signal with some additional high frequency noise. As a result of the geomagnetic field signal being artificially inserted into the magnetometer readings, we are able to calculate the RMSE and Pearson Correlation Coefficient with respect to the original signal. The results for the original, decimated, and moving-mean signals are shown in the following table.

Metrics				
	50 Hz	10 Hz	1 Hz	Moving Mean (N=10)
ρ	0.979	0.995	0.98	00.995
RMSE	14.7 nT	7.26 nT	3.73 nT	6.91 nT
NRMSE	3.37%	1.66%	0.85%	1.58%

4 Discussion

In this study, we introduced a signal processing algorithm based on UBSS and demonstrated the separation of magnetic noise from geomagnetic field data. In the first experiment, we separated four noise signals from a sine wave representing a ULF wave in simulation. The noise signals contained both sparse sine wave signals and wideband sawtooth and square wave signals. The algorithm was able to restore the ULF signal with a correlation coefficient of $\rho = 0.9998$ and RMSE of 10.22 nT. The extremely high correlation coefficient and 10.22 nT RMSE suggests that the reconstructed ULF signal matches the true signal with a slight difference in amplitude. The amplitude of the original signal is 454 nT, which would result in an RMSE of 0.1 nT if the amplitudes of the true and reconstructed signals were equal. In the second experiment, we created four magnetic noise signals using copper coils to generate real magnetic field data and placed PNI RM3100 magnetometers with the bus of a CubeSat apparatus. Magnetic residual data was taken from the SWARM mission and artificially inserted into the magnetometer data. This experiment mimicked the computer simulated experiment, with two sparse noise signals and two wideband noise signals. The signal separation algorithm was executed

using several additional preprocessing techniques such decimating the sampling rate and applying a moving mean to the magnetometer data. The lowest RMSE of 3.72 nT was achieved by decimating the sample rate to 1 Hz. At 1 Hz, the PNI RM3100 magnetometer is rated to have a measurement error of X nT due to instrument noise. This result places the reconstruction error near the noise floor of the magnetometer. These results show that the proposed UBSS algorithm is an effective at removing spacecraft noise from magnetic field data.

In general, it is not feasible to adaptively cancel spacecraft noise when a single magnetometer is used. Adaptive noise cancellation requires the removal of noise signals that are time variable. The use of a single magnetometer requires that spacecraft noise be carefully characterized before launch. Otherwise, a change in spacecraft behavior may require special maneuvers to recharacterize noise signatures in situ (Miles et al., 2019). The use of multiple magnetometers allows for the discovery of noise signals through the comparison of magnetometer data. Sheinker and Moldwin (2016), Deshmukh et al. (2020) Imajo et al. (2021) each propose algorithms for noise cancellation using multiple magnetometers. The algorithm proposed by Sheinker and Moldwin (2016) is powerful at removing a single noise signal, but is not designed for multiple noise signals. Imajo et al. (2021) propose the use of ICA which is also limited by how many noise signals it can remove. ICA requires that the number of noise signals be the same or less than the number of magnetometers. Spacecraft contain many electrical systems that could generate magnetic interference, so this condition is rarely met. The advantage of the proposed UBSS algorithm over Imajo et al. (2021) and Sheinker and Moldwin (2016) is that it can cancel noise signals in an underdetermined system. This means that there are more noise signals present than magnetometers. This property of the algorithm provides the flexibility necessary to be applied to many different spacecraft without prior characterization of spacecraft noise. Finally, Deshmukh et al. (2020) designed a state estimation algorithm to translate housekeeping data to magnetic noise signals. Housekeeping currents provide an incomplete mapping of the distribution of currents within a spacecraft. This algorithm requires that the user have prior knowledge of the spacecraft in order to create transfer functions to model noise signals. The advantage of the proposed UBSS algorithm over this approach is that it is a blind signal processing algorithm. It requires no prior knowledge of the noise signals being removed.

The proprosed algorithm functions on the assumption that the noise signals are sparse, meaning that only one noise signal is present at a time or frequency. This is almost never true in the time domain, so we analyze the signals in the time-frequency domain. If a signal is not sparse, then its mixing vector cannot be accurately estimated by cluster analysis. Compressive sensing also requires sparsity in order to accurately reconstruct the separate signals. However, in this work we only wish to reconstruct the geomagnetic field signal with high fidelity. Hence, we do not care if two noise signals overlap with each other so long as they do not overlap with the geomagnetic field signal present equally at each magnetometer.

In both experiments, we use sawtooth and square waves to test the cancellation of wideband signals. However, a signal commonly found in magnetomter data that we did not analyze is an spike that might be created from an electrical system rapidly turning on and off. Spike-shaped noise signals inhabit a very large frequency spectrum and diminish signal sparsity. In this case, it might be possible to use the proposed signal processing algorithm in combination with other processing algorithms such as median filtering or another spike filtering algorithm (Chandra et al., 1998).

The proposed algorithm requires that several parameters be set by the user. In this study, the parameters were manually selected based on the signals being analyzed, but this process could also be automated. The first parameter is the quality factor, Q. This parameter adjusts the window size used in the Non-Stationary Gabor Transform. We experimentally selected it, but it may be chosen based on the length of the signal be-

ing processed. The parameter, λ, is used to remove low energy noise signals. Data points that are below a fraction, λ, of the maximum energy data point are removed before clustering occurs. We selected this parameter by analyzing the data projected onto the half-unit hypersphere in Figure 2, and visually observing if the the signals were clusterable. If λ is too small, then the hypersphere will be completed filled with data points, and the noise signals will not be discoverable. If λ is too large, then small noise signals may not appear at all. Lastly, DBSCAN requires that two parameters, *eps*, and *MinPts*, be selected. The parameter, *eps*, represents the maximum distance allowed for two datapoints to be considered neighbors. The parameter, *MinPts*, represents the number of neighbors required for a data point to be considered a core. *MinPts* may be selected based on the length of signal being processed. A disadvantage of using NSGT and DBSCAN together is that more data points are created for higher frequency signals because the window size is altered based on frequency. Therefore, *MinPts* should be selected based on the lower frequency signals.

There are several avenues of development for future development of this algorithm. The most immediate step to be taking is for the selection of parameters to be automated. We present an algorithm to automate the noise cancellation process, but some rudimentary analysis is still required to select clustering and pre-processing parameters. We believe this process could be entirely automated. Another avenue of development is to test the limits of the sparsity assumption. Sparsity is a very strict assumption that may not always be met. In this work, we tested the algorithm using several wideband signals. However, the threshold for minimum sparsity is unknown. Finally, an interesting scenario to investigate is where several magnetometers are mounted within the bus of a spacecraft, but one magnetometer is mounted on a short boom, such as on the spacecraft Dellingr. In this scenario, the readings of one magnetometer may be more accurate than the others. It would be counter effective if the reconstructed magnetometer signal had more noise than the signal measured by the magnetometer on the boom. It may be possible to account for this by designing a programmable "faith" parameter at the compressive sensing stage. This variable would indicate an elevated degree of trust in one magnetometer over the others.

Explorer class missions, which perform world-class scientific investigations, require less than 2 nT error (Citation Needed). The lowest error achieved in this experiment is 3.73 nT. This error is near the expected measurement noise for the PNI RM3100 magnetometer. Further experimentation is needed to evaluate the ratio of signal reconstruction error to instrument noise, and investigate if the algorithm is suitable for explorer class missions. Nevertheless, the experiments performed show successful reconstruction of magnetic perturbation signals measured from within the bus of a mock CubeSat. These results prove the utility of boomless CubeSats for scientific investigation of magnetic field phenomena in the geospace environment. In turn, the low cost of CubeSats enables the use of large constellations of small satellites to measure the geomagnetic field with high temporal and spatial resolution.

5 Conclusion

In this study, we have proposed an algorithm for separating spacecraft generated magnetic noise signals from geomagnetic field data using multiple magnetometers. The algorithm does not require knowledge of the number of noise sources or types of noise signals. This algorithm identifies signals by looking at the relative gain and phase of the magnetometer signals in the Time-Frequency domain. If a noise signal is sparse in this domain, the relative gain and phase is found using cluster analysis. Following the same assumption of sparsity, the signal can be separated from the noisy data using the cluster centroids in compressive sensing.

The algorithm is designed for underdetermined systems in which there are more noise sources than magnetometers. An advantage of this approach is that the UBSS algorithm can can be integrated onto any satellite since no prior characterization or information of noise signals is required. This design eases the

We performed two experiments to validate this algorithm. The first experiment used computer simulated signals, and was able reconstruct five noise signals with an RMSE of 8 nT and a correlation of $\rho \approx 0.999$ each. The second experiment used real magnetic noise signals generated by copper coils, and residual geomagnetic field data. This experiment was able to separate four noise signals and reconstruct the background magnetic perturbations with a RMSE of 7.26 nT and a correlation of $\rho = 0.995$ at a 10 Hz cadence.

These results show that the potential of signal processing algorithms to ameliorate the presence of electrical noise in spaceborne magnetometer data. If a spacecraft can be designed to generate magnetic noise with non-overlapping spectral properties, this algorithm enables the possibility of lowcost, boomless spacecraft to capture high fidelity magnetic field measurements.

References

Baraniuk, R. G. (2007, July). Compressive Sensing [Lecture Notes]. *IEEE Signal Processing Magazine*, *24*(4), 118–121. (Conference Name: IEEE Signal Processing Magazine) doi: 10.1109/MSP.2007.4286571

Chandra, C., Moore, M., & Mitra, S. (1998). An efficient method for the removal of impulse noise from speech and audio signals. In *ISCAS '98. Proceedings of the 1998 IEEE International Symposium on Circuits and Systems (Cat. No.98CH36187)* (Vol. 4, pp. 206–208). Monterey, CA, USA: IEEE. Retrieved 2021-12-13, from `http://ieeexplore.ieee.org/document/698795/` doi: 10.1109/ISCAS.1998.698795

Deshmukh, A. A., Sharma, S., Cutler, J. W., Moldwin, M., & Scott, C. (2020, February). Simple Regret Minimization for Contextual Bandits. *arXiv:1810.07371 [cs, stat]*. Retrieved 2021-07-23, from `http://arxiv.org/abs/1810.07371` (arXiv: 1810.07371)

Diamond, S., & Boyd, S. (n.d.). CVXPY: A Python-Embedded Modeling Language for Convex Optimization. , 5.

Domahidi, A., Chu, E., & Boyd, S. (2013, July). ECOS: An SOCP solver for embedded systems. In *2013 European Control Conference (ECC)* (pp. 3071–3076). Zurich: IEEE. Retrieved 2021-08-18, from `https://ieeexplore.ieee.org/document/6669541/` doi: 10.23919/ECC.2013.6669541

Fratter, I., Léger, J.-M., Bertrand, F., Jager, T., Hulot, G., Brocco, L., & Vigneron, P. (2016). Swarm Absolute Scalar Magnetometers first in-orbit results. *Acta Astronautica*, *121*, 76–87. Retrieved from `https://www.sciencedirect.com/science/article/pii/S0094576515004671` doi: https://doi.org/10.1016/j.actaastro.2015.12.025

He, X.-s., He, F., & Xu, L. (2021, March). Underdetermined mixing matrix estimation based on joint density-based clustering algorithms. *Multimedia Tools and Applications*, *80*(6), 8281–8308. Retrieved 2021-07-07, from `https://doi.org/10.1007/s11042-020-10102-5` doi: 10.1007/s11042-020-10102-5

Imajo, S., Nosé, M., Aida, M., Matsumoto, H., Higashio, N., Tokunaga, T., & Matsuoka, A. (2021, May). Signal and Noise Separation From Satellite Magnetic Field Data Through Independent Component Analysis: Prospect of Magnetic Measurements Without Boom and Noise Source Information. *Journal of Geophysical Research: Space Physics*, *126*(5). Retrieved 2021-06-30, from `https://onlinelibrary.wiley.com/doi/10.1029/2020JA028790` doi: 10.1029/2020JA028790

Jaillet, F., Balazs, P., & Dorfler, M. (n.d.). Nonstationary Gabor Frames. , 4.

Kilcommons, L. M., Redmon, R. J., & Knipp, D. J. (2017). A new DMSP magnetometer and auroral boundary data set and estimates of field-aligned currents in dynamic auroral boundary coordinates. *Journal of Geophysical Research: Space Physics*, *122*(8), 9068–9079. Retrieved 2021-11-02, from https://onlinelibrary.wiley.com/doi/abs/10.1002/2016JA023342 (_eprint: https://onlinelibrary.wiley.com/doi/pdf/10.1002/2016JA023342) doi: 10.1002/2016JA023342

McMahon, P., Jung, H.-J., & Edwards, J. (2013, September). Swarm Deployable Boom Assembly (DBA) Development of a Deployable Magnetometer Boom for the Swarm Spacecraft. , *718*, 13. Retrieved 2021-08-19, from https://ui.adsabs.harvard.edu/abs/2013ESASP.718E..13M (Conference Name: 15th European Space Mechanisms and Tribology Symposium ADS Bibcode: 2013ESASP.718E..13M)

Miles, D. M., Howarth, A. D., & Enno, G. A. (2019, August). In situ calibration of offsetting magnetometer feedback transients on the Cassiope spacecraft. *Geoscientific Instrumentation, Methods and Data Systems*, *8*(2), 187–195. Retrieved 2021-07-31, from https://gi.copernicus.org/articles/8/187/2019/ (Publisher: Copernicus GmbH) doi: 10.5194/gi-8-187-2019

Naik, G., & Kumar, D. (2009, December). Determining Number of Independent Sources in Undercomplete Mixture. *EURASIP J. Adv. Sig. Proc.*, *2009*. doi: 10.1155/2009/694850

Regoli, L. H., Moldwin, M. B., Pellioni, M., Bronner, B., Hite, K., Sheinker, A., & Ponder, B. M. (2018, March). Investigation of a low-cost magneto-inductive magnetometer for space science applications. *Geoscientific Instrumentation, Methods and Data Systems*, *7*, 129–142. Retrieved 2021-11-25, from https://ui.adsabs.harvard.edu/abs/2018GI.....7..129R (ADS Bibcode: 2018GI.....7..129R) doi: 10.5194/gi-7-129-2018

Sheinker, A., & Moldwin, M. B. (2016, February). Adaptive interference cancelation using a pair of magnetometers. *IEEE Transactions on Aerospace and Electronic Systems*, *52*(1), 307–318. (Conference Name: IEEE Transactions on Aerospace and Electronic Systems) doi: 10.1109/TAES.2015.150192

Sun, J., Li, Y., Wen, J., & Yan, S. (2016, January). Novel mixing matrix estimation approach in underdetermined blind source separation. *Neurocomputing*, *173*, 623–632. Retrieved 2021-08-17, from https://www.sciencedirect.com/science/article/pii/S092523121501142X doi: 10.1016/j.neucom.2015.08.008